

A LOOK AT GENERAL CAVITY THEORY THROUGH A CODE
INCORPORATING MONTE CARLO TECHNIQUES

A Thesis

by

MARK DUFFY WEYLAND

Submitted to the Office of Graduate Studies of
Texas A&M University
in partial fulfillment of the requirements for the degree of

MASTER OF SCIENCE

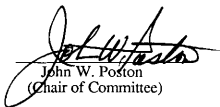
December 1989

Major Subject: Health Physics


A LOOK AT GENERAL CAVITY THEORY THROUGH A CODE
INCORPORATING MONTE CARLO TECHNIQUES

A Thesis
by
MARK DUFFY WEYLAND

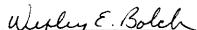
Approved as to style and content by:



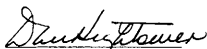
John W. Poston
(Chair of Committee)



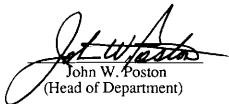
Gerald A. Schlapper
(Member)



Wesley E. Bolch
(Member)



Dan Hightower
(Member)



John W. Poston
(Head of Department)

December 1989

ABSTRACT

A Look at General Cavity Theory Through a Code Incorporating

Monte Carlo Techniques. (December 1989)

Mark Duffy Weyland, B. S., Texas A&M University;

Chair of Advisory Committee: Dr. John Poston

General cavity theory is used to relate the absorbed doses in two different media. A thermoluminescent dosimeter (TLD), which measures an absorbed dose in a medium different from its own sensitive volume, has its dose related to that medium using cavity theory. The most widely accepted cavity theory was introduced by T.E. Burlin (1966), and has an important assumption associated with it: the electrons from one material, the wall, being exponentially attenuated into the dosimeter, or the cavity. This assumption was investigated in this research using the Monte Carlo techniques in a modern computer code EGS4. Appropriate geometries were defined in the code and a sufficient number of photon histories were run to achieve statistical significance. The Monte Carlo results obtained for wall materials with low Z numbers and densities matched well with the theory of Burlin. For wall materials with high Z numbers and densities, however, the Monte Carlo results showed a significantly higher ratio of cavity dose to wall dose. This is believed to be caused by backscatter into the cavity which is not considered in the theory.

ACKNOWLEDGEMENTS

I would like to extend a special thanks to Dr. John W. Poston, my committee chairman, whose strive for excellence can't help but inspire those around him. He has been a good friend, whose high standards and continuous success in life will always give me the initiative to set high goals in all my future endeavors.

I would like to thank the rest of my graduate committee, Dr. Gerald A. Schlapper, who always has a good word of advice, Dr. Dan Hightower, who showed me a fascinating different view of health physics, and Dr. Wesley Bolch, whose youth and energy seems to relate better to the graduate students.

A very special thanks is extended to Mr. Gamal Akabani. Without his unending patience, and his strong support, this project might have taken much longer than it did.

My sincere appreciation goes out to my parents, Charles and Joyce Weyland, for their unwavering belief in my abilities for graduate studies. I would also like to thank my sisters, Kelley and Becky Weyland. Kelley has shown me that organization and neatness can make life easier; and Becky, by her own example, never lets me forget to have fun and not take life too seriously.

Finally, I would like to extend my warmest appreciation to Staci, whose unending love, support, and confidence in my ability help carry me through it all.

DEDICATION

To my parents, Charles Duffy and Joyce Weyland, who, without reservation, gave me love, support, and the willingness to excel in order to achieve a worthy goal.

TABLE OF CONTENTS

	Page
ABSTRACT	iii
ACKNOWLEDGEMENTS	iv
DEDICATION	v
TABLE OF CONTENTS	vi
LIST OF FIGURES	vii
LIST OF TABLES	ix
CHAPTER	
I INTRODUCTION.....	1
II BACKGROUND.....	4
BRAGG - GRAY.....	4
SPENCER - ATTIX.....	8
BURLIN.....	13
III DEVELOPMENT.....	19
EGS4 AND CAVITY THEORY.....	19
PROCEDURE.....	21
IV RESULTS.....	33
V CONCLUSIONS.....	42
FUTURE WORK.....	44
REFERENCES.....	46
APPENDIX	
A. EGS4 SUBROUTINES.....	48
B. RESULT DATA.....	58
VITA.....	69

LIST OF FIGURES

Figure	Page
2.1 A fluence F of charged particles is shown crossing and interface between media w and g	5
2.2 A fluence F of charged particles passes through a thin layer of medium g sandwiched between regions containing medium w	7
2.3 The cavity - size transition in Burlin theory	13
2.4 Illustration of the exponential - decay and - buildup assumption in the Burlin cavity theory	15
3.1 Flow chart of EGS4.....	20
3.2 Cross - section of the wall and cavity inside the Monte Carlo code, EGS4	21
3.3 Two dimensional view of the layers created by geometric arrays used by EGS4.....	22
3.4 Dose profile, or energy deposition profile, in an Al - LiF - Al configuration with the photons entering from the left side of the figure.....	27
3.5 Dose profile, or energy deposition profile, in a C - LiF - C configuration with the photons entering from the left side of the figure.....	28
3.6 Dose profile, or energy deposition profile, in an A-150 - LiF - A-150 configuration with the photons entering from the left side of the figure	29
3.7 Dose profile, or energy deposition profile, in a Cu - LiF - Cu configuration with the photons entering from the left side of the figure.....	30
3.8 Dose profile, or energy deposition profile, in a Pb - LiF - Pb configuration with the photons entering from the left side of the figure.....	31
4.1 f Values - Aluminum, Theory vs. Monte Carlo.....	34
4.2 f Values - A - 150, Theory vs. Monte Carlo	35
4.3 f Values - Carbon, Theory vs. Monte Carlo.....	36
4.4 f Values - Copper, Theory vs. Monte Carlo.....	37
4.5 f Values - Lead, Theory vs. Monte Carlo.....	38

Figure	Page
4.6 Representation of backscatter in an Al - LiF - Al configuration.....	40
4.7 Representation of backscatter in a Pb - LiF - Pb configuration	41

LIST OF TABLES

Table		Page
2.1	Approximate Values of $R(T_0, T) = \Phi_{T^e, \delta} / \Phi_{T^e}$, the Ratio of the Differential Electron Fluences with and without δ - rays	10
2.2	Values of D_B/D_w Calculated for Air Cavities, Spencer Cavity Theory vs. Bragg - Gray Theory.....	12
3.1	t_{max} / R_{CSDA} as Calculated by Spencer (1959) for a Plane Perpendicular Source of Electrons of Incident Energy T_0	24
3.2	Maximum Penetration Depth, t_{max} , of Different Materials for Photon Energies 0.5 to 1.5 MeV	24
4.1	Quantitative Comparison of f Values for various media; Monte Carlo vs. Theory	33

CHAPTER I

INTRODUCTION

Measurement of the absorbed dose in a medium exposed to ionizing radiation requires the introduction of a radiation sensitive device into that medium (Burlin, 1968). This device usually is composed of a material different from the medium in terms of atomic number and density and will be referred to as a "cavity". Patterns of energy deposition in the medium will therefore differ from those in the cavity. Cavity theory is used to relate the absorbed dose in a cavity to that in the surrounding medium.

A dosimeter responds to the absorbed dose inside its sensitive volume. This sensitive volume is surrounded by some type of container which protects it from the outside elements, including light. When the primary radiation field is mostly indirectly ionizing radiation, this wall also serves as the medium in which the radiation may interact to create the secondary charged particles which reach the sensitive volume. If the wall is at least as thick as the maximum secondary charged-particle range, the response of a dosimeter will result only from secondary charged particles originating both in the wall and in the sensitive volume itself. If the wall and the sensitive volume are of the same composition, charged particle equilibrium (CPE) may exist in the sensitive volume (Ogunleye et al., 1980). Charged particle equilibrium being the state when for every charged particle of a given type and energy leaving the volume, there is an identical charged particle of the

same energy entering (Attix, 1986). When the materials are not the same, however, the dose in the sensitive volume, or cavity, depends on the relative fluence of charged particles originating in the wall. If the dosimeter is small, with respect to the range of the secondary charged particles, the dose to the sensitive volume may be assumed to be caused solely by particles originating in the wall, and thus the sensitive volume does not perturb the charged particle flux crossing it. The original Bragg - Gray cavity theory, along with modifications by Spencer and Attix, apply to this situation (Spencer et al., 1955). In most cases, however, current dosimeters do not meet the assumptions made in these theories. T.E. Burlin was the first to address the problem of a larger sensitive volume or cavity (Burlin, 1966). The main difference between the Burlin theory and the Bragg et al. theories is the parameter d . This parameter is a weighting factor which eliminates the cavity size restriction and, thus, is a critical variable. This parameter is dimensionless and depends on the depth of penetration in the cavity of the electrons produced in the wall. Burlin assumed the electron attenuation to be exponential. This assumption and the weighting factor, d , was investigated and tested in this research using a Monte Carlo electron transport code.

Cavity theory is used to determine the absorbed dose in a material which differs in composition to that of the dosimeter's sensitive volume. Knowing the absorbed doses in different materials is extremely important. First, the sensitive volume of a dosimeter is not tissue, and does not match it perfectly. This alone is reason enough to test the validity of cavity theory. There are also researchers, engineers, and scientists who have the need to know the absorbed dose in other materials for their own research or applications. Since the only way at present to determine the dose in a different material is to use a dosimeter and relate the measured dose to that within the material, Monte Carlo

techniques have been used to simulate the irradiation of various materials. The computer code EGS4 uses Monte Carlo techniques to simulate the randomness of radiation interactions with random number generators and can be used to transport photons and electrons with great spatial detail in any material or compound. Utilizing this code, the energy deposited, and thus the dose, may be estimated in any material or compound without using a dosimeter. This research will find the doses in many materials and in a commonly used dosimeter materials in order to relate them and compare them to values given by cavity theory. This will be expressed through the parameter f , which in cavity theory is an uncertain quantity because of an assumption made in the theory. This assumption is represented by the parameter d , which is incorporated into the theoretical f equation. Thus, a comparison of f values will test the assumption made in d .

In summary, this research will involve the application of modern computer techniques to the study of cavity theory. Although a number of modifications to the original theory have been proposed, this investigation will focus on those modifications suggested by Burlin (Burlin, 1966). The specific objectives of this research are as follows: 1) set up the appropriate geometries inside a suitable Monte Carlo radiation transport code, 2) follow a sufficient number of photon histories through selected wall materials to obtain results with a statistical significance, 3) track energy depositions throughout the cavity and wall, and 4) analyze the results and compare them to published theoretical values.

CHAPTER II

BACKGROUND

BRAGG - GRAY

The relation between absorbed doses of two different media is not a new problem. In 1910, W.H. Bragg qualitatively discussed the problem (Bragg, 1910). However, it wasn't until 1929 that L.H. Gray made quantitative statements concerning cavity ionization theory (Gray, 1929, 1936). He proved that a gas - filled cavity did not perturb the electron spectrum if the cavity was small enough with respect to the range of the electrons. Many investigations have studied the original Bragg - Gray theory and have suggested modifications. The most important of these are those of Spencer and Attix, and Burlin (Spencer and Attix, 1955, Burlin, 1966). The following paragraph contains Burlin's (1968) assessment of the Bragg - Gray relation.

"Take into consideration two volumes, one being a solid throughout and one containing a small gas - filled cavity. Let the ratio of the dimensions of the gas-filled volume to those of the solid volume be in the ratio $s:1$. The constant of proportionality, s , is set equal to the ratio of the electron stopping powers of the solid and the gas. This was to ensure that electrons crossing the two volumes with corresponding paths would lose the same amount of energy. The number of electrons crossing the gas chamber will be s^2 times the number of electrons crossing the solid volume because of the larger cross sectional area of the gas cavity. The gas volume however is s^3 times that of the solid volume and therefore the energy lost by the electrons per unit volume in the gas cavity is $1/s$ times the energy lost by the electrons per unit volume in the solid volume element."

Thus the principle of equivalence may be stated as: "The energy lost per unit volume by electrons in the cavity is $1/s$ times the energy lost by γ rays per unit volume of the solid" (Gray, 1936; Burlin, 1968). Then it must follow that the energy absorbed per unit

volume in the gas cavity is 1/s times the energy absorbed per unit volume in the solid.

The original Bragg - Gray relation is based on these theories and is seen in Eq. 2.1

(Burlin, 1968):

$${}_m s = \frac{{}_m E}{{}_m J} W \quad , \quad \text{Eq. 2.1}$$

where ${}_m s$ = the ratio of the mass stopping power of the solid to that of the gas,

${}_m E$ = the energy absorption per unit mass in the solid,

${}_m J$ = ionization per unit mass in the gas, and

W = average energy dissipated in the gas per ion pair formed.

To relate this to an absorbed dose, assume a fluence Φ of identical charged particles of kinetic energy T which pass through an interface between two different media, g and w , as seen in Fig. 2.1 (Attix, 1986).

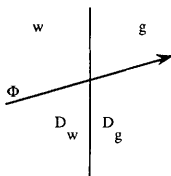


Fig. 2.1 A fluence Φ of charged particles is shown crossing an interface between media w and g . Assuming Φ to be continuous across the boundary, the dose ratio D_g/D_w equals the corresponding ratio of mass collision stopping powers. (Adapted from Attix, 1986)

The following can be written describing the absorbed doses on the g and w sides of the boundary, respectively:

$$D_g = \Phi \left[\left(\frac{dT}{\rho dx} \right)_{c,g} \right]_T, \quad \text{Eq. 2.2}$$

$$D_w = \Phi \left[\left(\frac{dT}{\rho dx} \right)_{c,w} \right]_T, \quad \text{Eq. 2.3}$$

where $[(dT/\rho dx)_{c,g}]_T$ and $[(dT/\rho dx)_{c,w}]_T$ are the mass collision stopping powers of the two media, evaluated at energy T (Attix, 1986). Since one of the conditions necessary for the Bragg - Gray relation to hold is that the fluence remain unperturbed, the constant Φ may be omitted in the ratio for the two absorbed doses. The energy T will be the same for both regions as well and thus will be left out of the ratio as seen in Eq. 2.4:

$$\frac{D_w}{D_g} = \frac{(dT/\rho dx)_{c,w}}{(dT/\rho dx)_{c,g}}. \quad \text{Eq. 2.4}$$

Bragg (1910) and Gray (1929, 1936) applied this equation to the problem of relating the absorbed dose in a solid volume with the absorbed dose in a solid volume containing the gas - filled cavity (Attix, 1986). Assume a layer g, or cavity, is inserted into a homogeneous medium w, as seen in Fig. 2.2. The first and main condition of the Bragg - Gray relation is that the thickness of the g - layer is assumed to be so small in comparison with the range of the charged particles striking it that its presence does not perturb the charged - particle field (Attix, 1986).

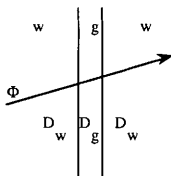


Fig. 2.2 A fluence Φ of charged particles passes through a thin layer of medium g sandwiched between regions containing medium w . Assuming Φ to be continuous across layer g and both interfaces, the dose ratio D_g/D_w is again equal to the corresponding ratio of mass collision stopping powers. (Adapted from Attix, 1986)

Another condition associated with the Bragg - Gray relation is that all charged particles must originate outside the cavity. Since the cavity is small enough so as not to perturb the charged particle flux crossing it, this may be stated as follows: the absorbed dose in the cavity is assumed to be deposited entirely by the charged particles crossing it (Attix, 1986). Using these two conditions, the ratio of absorbed dose to the wall to that of the cavity is given by Eq. 2.4. For a differential energy distribution Φ_T (particles per cm^2 per MeV) the appropriate average mass collision stopping power in the cavity medium g is (Attix, 1986):

$$\bar{S}_g = \frac{\int_0^{T_{\max}} \Phi_T \left(\frac{d\Gamma}{\rho dx} \right)_{c,g} d\Gamma}{\int_0^{T_{\max}} \Phi_T d\Gamma} = \frac{1}{\Phi} \int_0^{T_{\max}} \Phi_T \left(\frac{d\Gamma}{\rho dx} \right)_{c,g} d\Gamma = \frac{D_g}{\Phi} \quad , \quad \text{Eq. 2.5}$$

and likewise, for a thin layer of wall material w ,

$$m\bar{S}_w = \frac{\int_0^{T_{\max}} \Phi_T \left(\frac{dT}{\rho dx} \right)_{c,w} dT}{\int_0^{T_{\max}} \Phi_T dT} = \frac{1}{\Phi} \int_0^{T_{\max}} \Phi_T \left(\frac{dT}{\rho dx} \right)_{c,w} dT = \frac{D_w}{\Phi} \quad \text{Eq. 2.6}$$

Finally, by combining equations 2.5 and 2.6, the Bragg - Gray relation can be expressed terms of absorbed dose:

$$\frac{D_w}{D_g} = \frac{m\bar{S}_w}{m\bar{S}_g} = m\bar{S}_g^w \quad \text{Eq. 2.7}$$

Important aspects of the Bragg - Gray relation are that it does not require charged-particle equilibrium (CPE) nor a homogeneous field of radiation; however, the charged - particle fluence Φ_T must be the same in the cavity and in the medium w at the place where D_w is to be determined (Attix, 1986).

SPENCER - ATTIX

L.V. Spencer and F.H. Attix realized that the Bragg - Gray relation did not take into account fast secondary electrons generated by electron - electron collisions, or δ rays (Spencer and Attix, 1955). It was shown through experiments that these electrons affected the results and the greatest variance from Bragg - Gray theory occurred when the cavity and wall atomic numbers were very different. One reason the Bragg - Gray theory proved to be inadequate is that the continuous slowing - down approximation (CSDA) was used for the collision stopping powers. The CSDA range does not take into account

energy loss from delta rays. Even though delta rays are a small fraction of the total collisions they represent a significant amount of the energy loss. Delta (δ) rays are in fact, energetic electrons originating from head-on electron - electron collisions. These electrons join the flux of electrons already crossing the cavity (Attix, 1955). These delta rays increase the electron spectrum at lower energies since, for example, the original electron may transfer 1/4 of its energy to the resulting δ ray (Attix, 1955).

The Spencer - Attix theory (Spencer and Attix, 1955; Spencer, 1965, 1971) has two general conditions: the existence of CPE and the absence of bremsstrahlung production (Attix, 1986). Their derivation specifically dealt with a distributed homogeneous source of monoenergetic electrons of initial energy T_0 (MeV) which emits N particles per gram throughout a homogeneous medium w . The cavity size was represented by the parameter Δ , and the electrons were given a mean energy having projected ranges just large enough to cross the cavity. The equilibrium spectrum of electrons and delta rays, Φ_T^e, δ , generated in the surrounding medium is arbitrarily divided into two components in the Spencer - Attix schematization (Attix, 1986):

- a.) The "fast" group: electrons which have energies $T \geq \Delta$ and are therefore able to transport energy. In particular, these electrons have enough energy to cross the cavity.
- b.) The "slow" group: electrons with $T < \Delta$. These are assumed to have zero range, i.e., are assumed to deposit their energy "on the spot" at which their kinetic energy falls below Δ . Hence, these electrons are assumed to be unable to enter the cavity or to transport energy.

The absorbed dose at any point in medium w , where CPE exists is given by (Attix, 1986):

$$D_w^{\text{CPE}} = N T_o = \int_{\Delta}^{T_o} \Phi_T^{e,\delta} {}_mS_w(T,\Delta) dT, \quad \text{Eq. 2.8}$$

where ${}_mS_w(T,\Delta)$ is the restricted stopping power for electrons of energy T in medium w , which includes only energy losses to δ rays below Δ . The equilibrium spectrum, $\Phi_T^{e,\delta}$, can be found using the following equation: (Attix, 1986)

$$\Phi_T^{e,\delta} = \frac{NR(T_o, T)}{(dT/\rho dx)_w}, \quad \text{Eq. 2.9}$$

where $R(T_o, T)$ is the ratio of the differential electron fluence including δ rays to that of primary electrons alone. Table 2.1, taken from Attix (1986), shows how the equilibrium spectrum is drastically increased as the electron energy becomes very small in comparison with the original electron energy. Again, this is due to δ rays which the Bragg - Gray theory did not consider.

Table 2.1 Approximate Values of $R(T_o, T) = \Phi_T^{e,\delta} / \Phi_T^e$, the Ratio of the Differential Electron Fluences with and without δ - rays (Adapted from Attix, 1986)

T / T _o	R(T _o , T)				
	C	Al	Cu	Sn	Pb
1.000	1.00	1.00	1.00	1.00	1.00
0.500	1.00	1.00	1.00	1.00	1.00
0.250	1.05	1.05	1.06	1.06	1.07
0.125	1.21	1.23	1.25	1.27	1.29
0.062	1.60	1.66	1.73	1.79	1.85
0.031	2.40	2.60	2.80	2.90	3.10
0.016	4.40	4.70	5.20	5.50	6.00
0.008	8.50	9.40	10.50	11.30	12.30
0.004	17.00	19.00	22.00	24.00	-

By incorporating Eq. 2.9 into Eq. 2.8 and by deriving a similar equation for D_g in the cavity, the following absorbed dose relationship can be found from the Spencer - Attix cavity theory:

$$\frac{D_g}{D_w} = \frac{\int_{\Delta}^{T_0} \frac{R(T_0, T)}{(dT/\rho dx)_w} m S_g(T, \Delta) dT}{\int_{\Delta}^{T_0} \frac{R(T_0, T)}{(dT/\rho dx)_w} m S_w(T, \Delta) dT} \quad \text{Eq. 2.10}$$

Table 2.2 gives values of D_g/D_w using the Spencer - Attix relation and compares these to those obtained from the Bragg - Gray theory. The range in the table below represents the relative cavity sizes with increasing range signifying an increasing cavity size.

As can be seen, the Bragg - Gray values correspond most closely with Spencer - Attix for the larger cavity sizes. The variation away from unity increases with a decreasing cavity size because of the influence of more δ rays (Attix, 1986). Even though the terms "increasing" and "decreasing" cavity sizes are being used here, it should be remembered that the cavities discussed in the preceding theories must be small enough so as not to perturb the charged-particle flux crossing them.

Table 2.2 Values of D_g/D_w Calculated for Air Cavities, Spencer Cavity Theory vs. Bragg - Gray Theory (Adapted from Attix, 1986)

Wall Medium	To (keV)	Δ (keV) = Range (mm) =	D_g/D_w							
			Spencer							Bragg Gray
			2.500 0.015	5.100 0.051	10.200 0.190	20.400 0.640	40.900 2.200	81.800 7.200		
C	1308		1.001	1.002	1.003	1.004	1.004	1.005	1.005	
	654		0.990	0.991	0.992	0.992	0.993	0.994	0.994	
	327		0.985	0.986	0.987	0.988	0.988	0.989	0.989	
Al	1308		1.162	1.151	1.141	1.134	1.128	1.123	1.117	
	654		1.169	1.155	1.145	1.137	1.131	1.126	1.125	
	327		1.175	1.161	1.151	1.143	1.136	1.130	1.134	
Cu	1308		1.456	1.412	1.381	1.359	1.340	1.327	1.312	
	654		1.468	1.421	1.388	1.363	1.345	1.329	1.327	
	327		1.485	1.436	1.400	1.375	1.354	1.337	1.353	
Sn	1308		1.786	1.694	1.634	1.592	1.559	1.535	1.508	
	654		1.822	1.723	1.659	1.613	1.580	1.551	1.547	
	327		1.861	1.756	1.687	1.64	1.602	1.571	1.595	
Pb	1308		-	2.054	1.940	1.865	1.811	1.770	1.730	
	654		-	2.104	1.985	1.904	1.848	1.801	1.796	
	327		-	2.161	2.030	1.946	1.881	1.832	1.876	

BURLIN

T.E. Burlin (1966) is credited with deriving an expression which could account for larger cavity sizes. Most dosimeters are too large and do not comply with the cavity size restrictions of the earlier theories. A theory relating absorbed dose in a wall to that of a cavity, or dosimeter, of any size allowed for more the accurate estimates of doses in any media. Attix (1986) illustrates the difference in cavity sizes in Fig. 2.3. In this figure, there is a homogeneous medium w with a uniform γ ray irradiation. All three cavities contain a medium g and are shown as: a) small (applicable for Bragg - Gray, and Spencer - Attix), b) intermediate, and c) large compared to the ranges of the secondary electrons present (Attix, 1986).

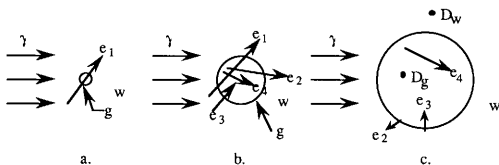


Fig. 2.3 The cavity - size transition in Burlin theory (Adapted from Attix, 1986).

The absorbed dose in the small cavity is almost completely delivered by secondary electrons completely crossing the cavity such as e_1 . In the intermediate sized cavity, the absorbed dose is partly due to secondary electrons such as e_1 , but also from electrons which originate in the cavity and stop in the wall such as e_2 , electrons which originate in

the wall and stop in the cavity such as e_3 , and from electrons which start and stop inside the cavity such as e_4 . If the cavity is large, with respect to the range of the secondary electrons, it should be clear that the majority of the absorbed dose would come from electrons such as e_4 which start and stop inside the cavity. The following list of assumptions made by Burlin in his 1966 paper were assembled by Attix (1986); these assumptions simplify the theory:

- 1.) The media w and g are homogeneous throughout, but are not necessarily of the same material.
- 2.) A homogeneous γ ray field exists everywhere throughout w and g .
(This means that no γ ray attenuation correction is made in this theory for the presence of the cavity.)
- 3.) Charged - particle equilibrium (CPE) exists at all points in w and g that are farther than the maximum electron range from the cavity boundary.
- 4.) The equilibrium spectra of secondary electrons generated in w and g are the same.
- 5.) The fluence of electrons entering from the wall is attenuated exponentially as it passes through the medium g , without changing the spectral distribution.
- 6.) The fluence of electrons that originate in the cavity builds up to an equilibrium value exponentially as a function of distance into the cavity, according to the same attenuation coefficient β that applies to the incoming electrons. This can be seen in Fig. 2.4 for the simple homogeneous case where $g = w$.

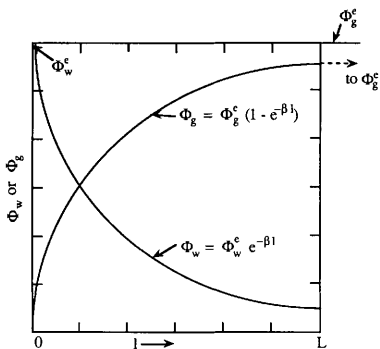


Fig. 2.4 Illustration of the exponential - decay and - buildup assumption in the Burlin cavity theory. The equilibrium wall fluence of electrons, Φ_w^e , is shown to be decreasing exponentially as a function of position in a homogeneous cavity for which the wall w and cavity g media are assumed to be identical. The electrons under consideration are only those flowing from left to right. The buildup of the cavity - generated electron fluence Φ_g follows a complementary exponential profile which, asymptotically approaches the equilibrium value $\Phi_g^e = \Phi_w^e$ (Adapted from Attix, 1986).

In its simplest form, the absorbed dose ratio, according to the Burlin theory, may be written as follows:

$$f = \frac{D_g}{D_w} = d \left[\frac{m \bar{S}_g}{m \bar{S}_w} \right] + (1 - d) \left[\frac{(\mu_{en}/\rho)_g}{(\mu_{en}/\rho)_w} \right], \quad \text{Eq. 2.11}$$

where:

f = ratio of absorbed dose in the cavity to that in the wall;

- D_g = absorbed dose in the cavity;
 D_w = absorbed dose in the wall;
 d = weighting factor for different cavity sizes;
 ${}_mS_g$ = average mass collision stopping power for the cavity;
 ${}_mS_w$ = average mass collision stopping power for the wall;
 $(\mu_{en}/\rho)_g$ = average mass energy - absorption coefficient for the cavity;
 $(\mu_{en}/\rho)_w$ = average mass energy - absorption coefficient for the wall.

The parameter d is the critical variable in this equation because it eliminates the cavity size restriction. It approaches zero for large cavities and unity for smaller ones. Other studies have looked at different cavity sizes and their effects on dose and have shown limited variation in f (Kearsley, 1984, Horowitz, 1986). This study will exclusively focus on a cavity the size of a standard TLD chip, which in Burlin's theory is a medium cavity and was calculated using the following equation as, $d = 0.514$. One of the assumptions Burlin made was that the secondary electrons would be attenuated exponentially, and d represents this assumption. He defined d as the mean of $\Phi_w/\Phi_w e$ in the cavity as expressed in Eq. 2.12 and seen in Fig. 2.4 (Attix, 1986):

$$d = \frac{\overline{\Phi_w^e}}{\Phi_w^e} = \frac{\int_0^L \Phi_w^e e^{-\beta l} dl}{\int_0^L \Phi_w^e dl} = \frac{1 - e^{-\beta L}}{\beta L} , \quad \text{Eq. 2.12}$$

- where: l = distance of any point in cavity from wall (cm);
 L = mean chord length (cm); and

β = attenuation coefficient (cm^{-1}).

The other parameters have been defined previously. The parameter L may be defined as 4 times the volume divided by its surface area, for convex cavities and diffuse (i.e. isotropic) electron fields (Attix, 1986). The attenuation coefficient, β , was defined by Burlin for air filled cavities as:

$$\beta = \frac{16 \rho}{(T_{\max} - 0.036)^{1.4}} , \quad \text{Eq. 2.13}$$

where: ρ = air density (g/cm^3);

T_{\max} = maximum value of the starting β ray energies (MeV).

In a later paper, Burlin et al. defined β as (Burlin et al., 1969):

$$\exp(-\beta R) = 0.01 , \quad \text{Eq. 2.14}$$

where R is the range obtained from the continuous slowing down approximation (R_{CSDA}) in $\text{g}\cdot\text{cm}^{-2}$. This parameter, β , was modified when detailed experiments were carried out with different materials. The expression obtained for LiF was (Paliwal, Almond, 1975):

$$\beta = \frac{14}{E_{\max}^{1.09}} \quad (\text{cm}^2/\text{g}) , \quad \text{Eq. 2.15}$$

where E_{\max} is the maximum electron energy in MeV. This expression was obtained by the method of linear regression which was applied to fit the data of E_{\max} . It should be

noted that even today there is controversy surrounding this parameter (Paliwal and Almond, 1975).

The Burlin theory along with the Bragg - Gray and Spencer - Attix theories all ignore electron scattering. Experiments by Ogunleye et al. (1980) seem to show that the Burlin theory comes very close to approximating the doses in various media. There have been many theories and published papers challenging the Burlin theory and its related parameters. Theories trying to match the data produced by Ogunleye et al. also have been published, but the simplicity of Burlin's theory and its seemingly close approximation of doses in different media warrant further study as to the accuracy of the actual doses.

CHAPTER III

DEVELOPMENT

EGS4 AND CAVITY THEORY

The Monte Carlo code used in this study is called EGS4 (Electron Gamma Shower 4). The EGS4 system of computer codes is a general purpose package for the Monte Carlo simulation of the coupled transport of electrons and photons in an arbitrary geometry for particles with energies above a few keV. The code can be used to follow detailed interactions including; Bremsstrahlung production, positron annihilation, Moliere and Bhabha scattering, continuous energy loss applied to charged particle tracks between discrete interactions, along with pair production, Compton scattering, and the photoelectric effect (Stanford Linear Accelerator Center, 1986). Transport of electrons or photons can be simulated in any element, compound, or mixture. Cross sections for materials of interest are prepared by the data preparation package, PEGS4, using cross section tables for elements 1 through 100. The geometry for any given problem is specified by the user - written subroutine HOWFAR. The user scores and outputs information in the user - written subroutine AUSGAB. Input parameters such as cutoff energies, photon energies, and wall thicknesses are read from the main program, MAINEGS4. MAINEGS4 has a data file called PATCLE, which also contains some user input parameters, such as photon energy, number of histories, and step size. A flow chart of EGS4 may be seen in Fig. 3.1 These subroutines may be seen in Appendix 1.

This code was modified to include a thermoluminescent dosimetry (TLD) chip cavity and a surrounding wall as thick as the maximum range of the secondary charged

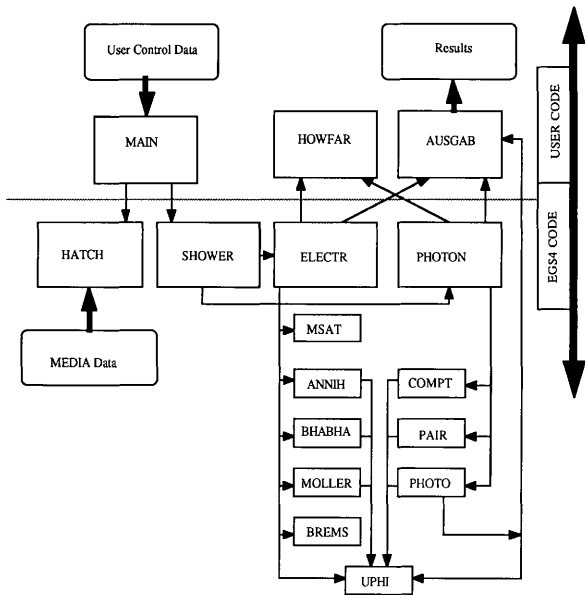


Fig. 3.1 Flow chart of EGS4 (Adapted from Stanford Linear Accelerator Center, 1986)

particles. A monoenergetic photon field was introduced on one side of the wall and energy deposition was tracked and recorded throughout the wall and cavity. The photon beam was directed perpendicular and at the geometrical center of the face of the wall where the photons impinged. This was a "pencil beam" of photons rather than a field of radiation. The method used was faster than the field of photons and test runs showed no deviation in results. Fig. 3.2 shows the geometry used in the EGS4 calculations. This is a cross sectional view, actually the wall completely surrounds the TLD chip cavity shown in the middle of the configuration.

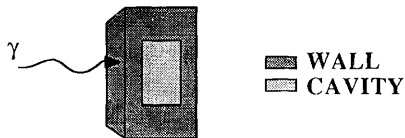


Fig. 3.2 Cross section of the wall and cavity inside of the Monte Carlo code, EGS4

Energy deposition in these regions was divided by the mass of the wall and cavity, respectively, to obtain absorbed doses. The cavity to wall dose ratio was obtained for four different energies ranging from 0.5 MeV to 1.5 MeV and five different materials: aluminum, copper, carbon, lead, and a tissue equivalent plastic, A-150.

PROCEDURE

As mentioned above, a cavity and wall were defined in the Monte Carlo code, EGS4, in three dimensions. The parameters for the cavity were the size of a standard Harshaw

TLD chip with dimensions 3.1 x 3.1 x 0.89 mm. The cavity was assumed to be composed of LiF, the same composition as the commonly used Harshaw TLD - 100. This cavity was divided into a 20 layers and then the layers were divided into 20 x 20

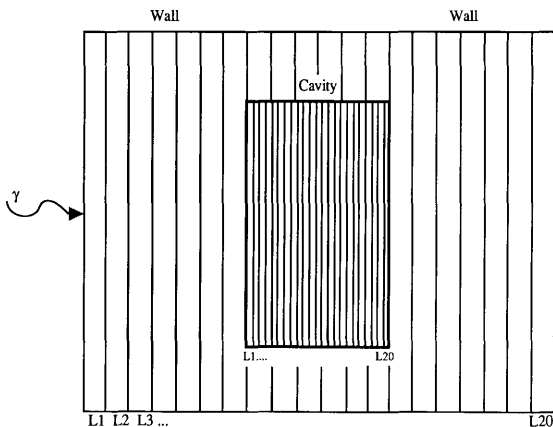


Fig. 3.3 Two dimensional view of the layers created by geometric arrays used by EGS4.

cubes using arrays in the subroutine AUSGAB for purposes of determining the locations of energy deposition. Figure 3.3 shows a cross section of the geometry inside of EGS4 with the arrays in place. The layers shown were used to determine the average energy deposition in the wall and cavity. The wall boundaries were as thick as the maximum

range of the secondary charged particles. A number of steps were taken to arrive at this distance.

First, it was assumed that, at photon energies of ≤ 0.5 MeV, the majority of the interactions were due to the photoelectric effect and thus the maximum kinetic energy, T_{\max} , of the resulting electron could be the same as the original photon. For photons ≥ 1 MeV, Compton scattering was assumed to be the main contributor, and thus the maximum kinetic energy, T_{\max} , of the resulting electron can be obtained from Eq. 3.1: (Attix, 1986)

$$T_{\max} = \frac{2 (h\nu)^2}{2 h\nu + 0.511 \text{ (MeV)}} \quad \text{Eq. 3.1}$$

Using T_{\max} , the continuous slowing down approximation ranges (R_{CSDA}) were found for the corresponding materials and energies (Attix, 1986). At this point, Table 3.1 was used to convert these ranges into the maximum penetration depth, t_{\max} , which is the distance beyond which no particles are observed to penetrate (Attix, 1986). For the purposes described here, this distance is the maximum range of the secondary charged particles.

Table 3.1 t_{\max}/R_{CSDA} as Calculated by Spencer (1959) for a Plane Perpendicular Source of Electrons of Incident Energy T_0 (Adapted from Attix, 1986)

$T_0(\text{MeV})$	Z = 6 (C)	13 (Al)	29 (Cu)	50 (Sn)	82 (Pb)
0.025	0.95	0.90	0.80	-	-
0.050	0.95	0.87	0.77	0.72	-
0.100	0.95	0.87	0.77	0.70	0.60
0.200	0.95	0.87	0.75	0.67	-
0.400	0.95	0.87	0.75	0.67	-
0.700	0.95	0.87	0.75	0.67	0.55
1.000	0.95	0.87	0.77	0.67	0.57
2.000	0.95	0.90	0.77	0.70	0.60
4.000	0.95	0.90	0.80	0.75	-
10.000	0.95	0.92	0.85	0.80	-

Since there were no correction factors available for A-150 plastic, the R_{CSDA} was used in place of t_{\max} . Since A-150 has a low effective atomic number, t_{\max} is comparable to R_{CSDA} (Attix, 1986). Table 3.2 shows the results of the above steps for the energies and

Table 3.2 Maximum Penetration Depth, t_{\max} , of Different Materials for Photon Energies 0.5 to 1.5 MeV

Photon Energy (MeV)	T_{\max}	t_{\max} (cm)				
		Al	C	Cu	Pb	A-150
0.50	0.500	0.0731	0.0902	0.0219	0.0178	0.1757
1.00	0.800	0.1360	0.1694	0.0412	0.0294	0.3300
1.25	1.038	0.1876	0.2352	0.0573	0.0411	0.4066
1.50	1.282	0.2436	0.3034	0.0734	0.0520	0.5915

materials used in this study. These parameters also were entered into the main program, MAINEGS4, and the surrounding wall, as with the cavity, was described in 20 layers and further by a 20 x 20 per layer array which formed cubes, for precise energy

deposition tracking. Figure 3.3 is a two dimensional view of the layers which were used for averaging the doses.

One hundred thousand photon histories were followed in each case to achieve high statistical accuracy. The energy deposited in every cube for all 100,000 photons was printed out along with a layer by layer energy deposition summary at the end of each case. It should be noted that because photons are being used here with relatively small thicknesses, part of the energy was carried through the configuration and escaped without depositing. In a real exposure, a similar loss of total energy would occur and, therefore, this result was expected. The absorbed dose is defined as energy per unit mass, so the energy deposited in each region was divided by the product of the cubical dimension, in cm^3 , and the respective material density, in g/cm^3 , to obtain the absorbed doses. The following is an example of the dose calculation described above; starting with energy depositions and determining the dose in units of MeV/g . This example is for 1.25 MeV photons impinging on an aluminum wall.

Example:

First, the energy deposition is summed over all layers in the cavity and divided by 20 to get an average layer energy deposition.

$$749.089 \text{ MeV} / 20 = 37.45 \text{ MeV}$$

This value is divided by the layer volume and the cavity (LiF) density to give a dose in units of MeV/g .

$$37.45 \text{ MeV} / (4.28\text{E-}4 \text{ cm}^3 * 2.64 \text{ g}/\text{cm}^3) = 33171.1 \text{ MeV}/\text{g}$$

This dose was divided by the dose to the wall, which was found by first taking the layer average of the energy depositions in the front wall after CPE had been established. That is, CPE is assumed to exist when the dose in the wall leveled off. This leveling off can be

seen for all the materials used in Figures 3.4 - 3.8. The dose in the following figures was normalized to 1 according to the highest dose in the front wall. This study is concerned with the relative doses in the wall and cavity and units are unnecessary. The energy deposition data used to calculate the dose profiles can be found in Appendix B which has the information for all the energies and materials used. These figures are typical of the energy deposition or dose profiles for the spectrum of energies used in this study. Since all the energy depositions per layer were divided by the same volume and density, the energy deposition profile would appear exactly the same as this dose profile. It should be noted that the dose in this figure was normalized to the highest dose in the front wall.

the average energy deposition in the wall material = 199.6 MeV

This was then divided by the layer volume and the density (Al in this case) to arrive at a dose.

$$199.6 / (.00223 \text{ cm}^3 * 2.69 \text{ g/cm}^3) = 33281.0 \text{ MeV/g}$$

The dose relationship, f , was then simply found by dividing the cavity dose by the wall dose as shown in Eq. 2.11 from the Background.

$$f = D_c / D_w = 33171.1 / 33281.0 = 0.99$$

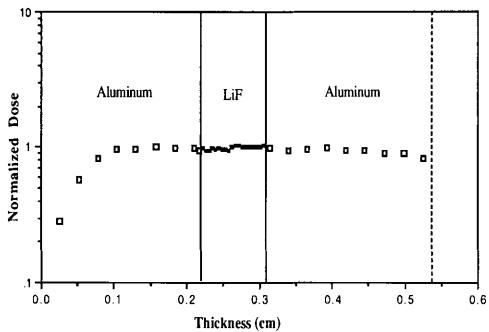


Fig. 3.4 Dose profile, or energy depositon profile, in an Al - LiF - Al configuration with the photons entering from the left side of the figure (1.25 MeV photons)

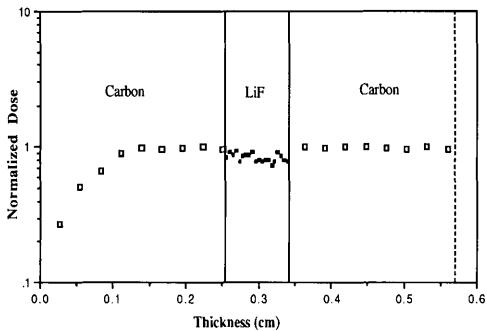


Fig. 3.5 Dose profile, or energy deposition profile, in a C - LiF - C configuration with the photons entering from the left side of the figure (1.25 MeV photons)

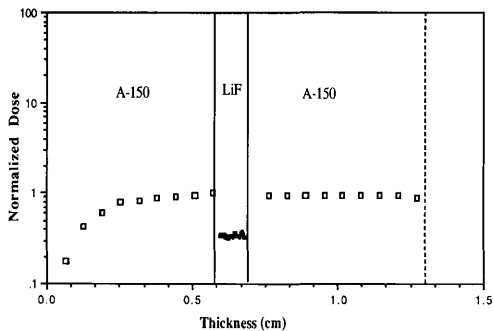


Fig. 3.6 Dose profile, or energy deposition profile, in an A-150 - LiF - A-150 configuration with the photons entering from the left side of the figure (1.25 MeV photons)

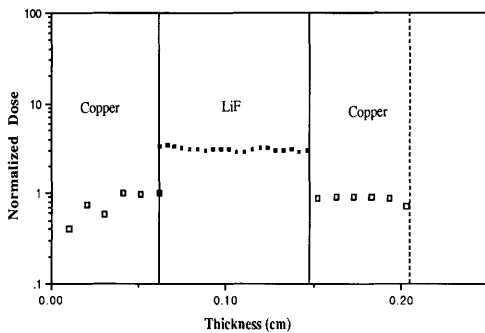


Fig. 3.7 Dose profile, or energy depositon profile, in a Cu - LiF - Cu configuration with the photons entering from the left side of the figure (1.25 MeV photons)

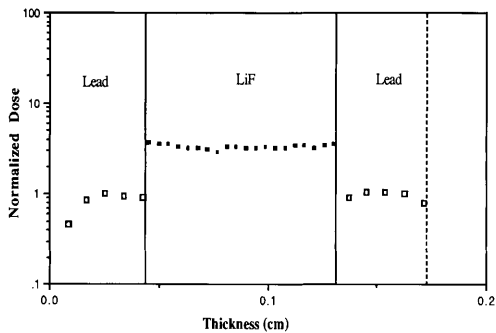


Fig. 3.8 Dose profile, or energy deposition profile, in a Pb - LiF - Pb configuration with the photons entering from the left side of the figure (1.25 MeV photons)

A theoretical estimate of f took many steps starting with Eq. 2.11. First the parameter d was calculated as according to Eq. 2.12. The parameters L , and β were needed for this calculation. As mentioned previously, L is defined as four times the volume divided by its surface area, and β is obtained from Eq. 2.15. After calculating d , the mass collision stopping powers and the mass energy - absorption coefficients were obtained by interpolation from tables for the appropriate energies (Attix, 1986). Again, using Eq. 2.11, the f values were calculated and compared to the values obtained from the Monte Carlo simulations. An example is shown below of the theoretical calculation for a 1.25 MeV photon in Aluminum.

Example calculation:

$$h\nu = 1.25 \text{ MeV}$$

Since the photon is above 1 MeV, Compton scattering is assumed to be the major interaction:

$$T_{\max} = 1.038 \text{ MeV}$$

$$T_{\max} = 2(h\nu)^2 / [2 h\nu + 0.511 \text{ MeV}] \text{ for Compton Scattering}$$

$$\beta = 13.44$$

$$\beta = 14 / T_{\max}^{1.09}$$

$$L = 0.1131$$

$$L = 4 \text{ Vol.} / \text{S.A.} \quad 0.31 \times 0.31 \times 0.089 \text{ (cm)}$$

$$d = 0.514$$

$$d = [1 - e^{-\beta L}] / \beta L$$

$$f = 0.989$$

$$f = d S_w^c + (1-d) (\mu_{en}/\rho)_w^c$$

CHAPTER IV

RESULTS

After analyzing the Monte Carlo data, and computing the theoretical values of f , a quantitative comparison of theory vs. Monte Carlo results was made. This comparison is shown in Table 4.1. Figure 4.1 shows a graphical comparison between the theory and Monte Carlo results in aluminum. Figures 4.2 - 4.5 present graphical comparisons between theory and Monte Carlo results in carbon, copper, lead, and A - 150 plastic, respectively.

Table 4.1 Quantitative Comparison of f Values for various media; Monte Carlo vs. Theory

Photon E (MeV)	f Values									
	Aluminum		Carbon		Copper		Lead		A - 150	
	Theory	M.C.	Theory	M.C.	Theory	M.C.	Theory	M.C.	Theory	M.C.
0.50	0.984	0.96	0.926	0.87	1.00	3.3	0.856	3.5	0.834	0.48
1.00	0.987	0.99	0.923	0.93	1.08	3.3	1.270	3.5	0.823	0.56
1.25	0.990	0.99	0.923	0.92	1.09	3.1	1.280	3.5	0.826	0.66
1.50	0.992	0.99	0.924	0.89	1.11	3.3	1.280	3.6	0.826	0.82

The results in the table above and in the following graphs show some agreement and some disagreement to the theory. Figures 4.1 - 4.5 graphically show the comparison of Monte Carlo results to values calculated through the theory. The values for aluminum correlate with theory as seen in Fig. 4.1. The slight variations fall well within the range for possible statistical differences. For the low Z materials, however, it was observed that, at low energies, Monte Carlo values had a slightly wider variation on the low side.

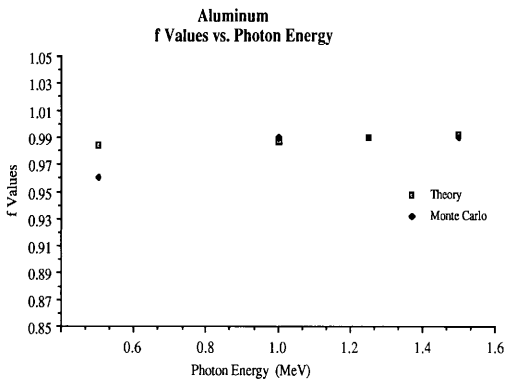


Fig. 4.1 f Values - Aluminum, Theory vs. Monte Carlo

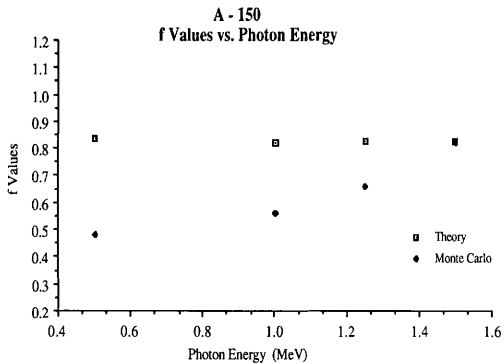


Fig. 4.2 f Values - A - 150, Theory vs. Monte Carlo

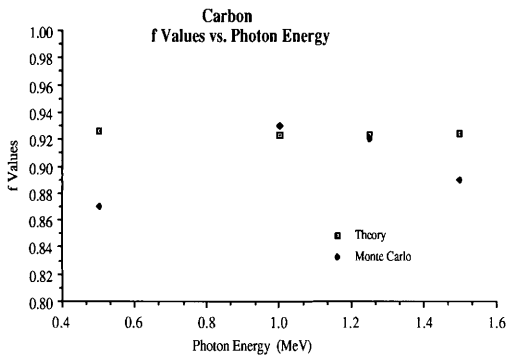


Fig. 4.3 f Values - Carbon, Theory vs. Monte Carlo

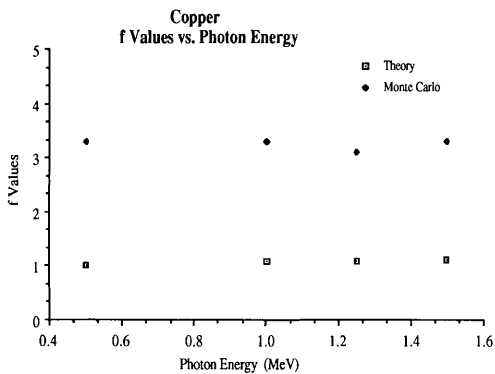


Fig. 4.4 f Values - Copper, Theory vs. Monte Carlo

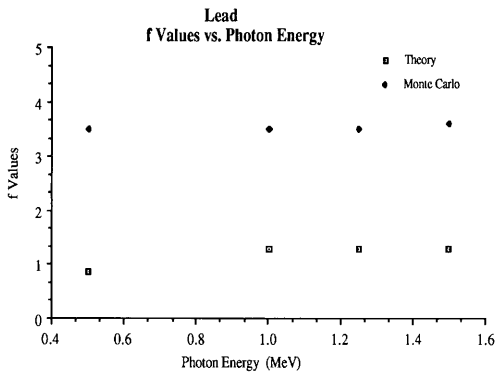


Fig. 4.5 f Values - Lead, Theory vs. Monte Carlo

For A - 150 plastic this variation is exaggerated as shown in Fig. 4.2. The carbon, Fig. 4.3, also agreed well with the theoretical calculations. These materials have relatively low Z numbers and densities. Take note that the scale representing the ordinate in graphs 4.1 - 4.5 is not the same for each graph. The next graph shows copper, Fig. 4.4, which has an unusually high density for its Z number. As can be seen, the Monte Carlo values are significantly higher by about a factor of 3. This is also observed in Fig 4.5, which is the lead comparison. These differences are believed to be caused by the much higher backscatter from the wall into the cavity associated with the denser, heavier elements. Figure 4.6 shows the backscatter of Co - 60 photons in an Al - LiF - Al configuration. This is represented by the small diagonal line at the bottom, right portion of the LiF cavity. Compare this to the much larger backscatter curve in Fig. 4.7, which represents a Pb - LiF - Pb configuration. This extra energy deposition would significantly increase the cavity dose, thus making the f value higher.

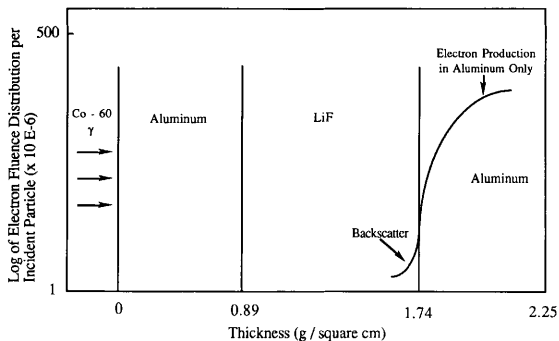


Fig. 4.6 Representation of backscatter in an Al - LiF - Al configuration (Adapted from Horowitz, 1986).

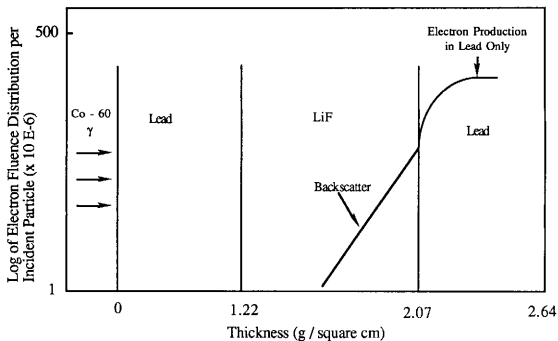


Fig. 4.7 Representation of backscatter in a Pb - LiF - Pb configuration (Adapted from Horowitz, 1986).

CHAPTER V

CONCLUSIONS

The goals of this project were to produce a Monte Carlo computer code with suitable geometries, run a sufficient number of photon histories for statistical significance, track energy depositions throughout the cavity and wall, and analyze the results and compare to theory. The first of these goals was accomplished by modifying an existing code, called EGS4. This code was developed at the Stanford Linear Accelerator Center (SLAC) and incorporates Monte Carlo techniques to transport and track photons and electrons. This code is capable of following detailed photon and electron interactions, including Bremsstrahlung production, positron annihilation, Moliere multiple scattering, Moller (e^-e^-) and Bhabha (e^+e^+) scattering, continuous energy loss applied to charged particle tracks between discrete interactions, along with pair production, Compton and Rayleigh scattering, and the photoelectric effect. A subroutine, HOWFAR, was written which defined a three dimensional cube and a three dimensional cavity inside of the cube. The cavity was the size of a standard TLD chip and was defined as LiF. The cube, or wall, was redefined for five different materials including aluminum, carbon, A - 150 plastic, copper, and lead. The wall thickness was defined as the maximum secondary charged particle range for reasons explained in the text.

One hundred thousand photon histories were run for each case insuring good statistics. These photons were tracked using a user written subroutine called AUSGAB. In this subroutine, the geometries, wall and cavity, were both broken down into $20 \times 20 \times 20$ arrays. This was done for precise tracking of the energy deposition in both regions.

The energy depositions were printed out for each material over a range of energies from 0.5 to 1.5 MeV.

These energy depositions were divided by the respective masses to obtain doses which could be compared to the theoretical absorbed dose values. The absorbed doses were actually compared to theory by using a ratio of cavity dose to wall dose represented by the parameter f . This parameter and the theoretical calculation of it is better explained in the Background chapter of this text. It was found that at low Z numbers, cavity theory yielded reasonably accurate doses, however, at high Z numbers and densities, cavity theory overestimated the doses to these heavier elements. It is fortunate that cavity theory overestimates the dose and is, thus, conservative. Nevertheless, it is incorrect. By using the results found here, other studies could be initiated defining the relationship between severely mismatched media.

The approximate 50% error seen with the A - 150 plastic between the theory and Monte Carlo values at the lowest energy, along with much smaller variations in the same direction for the two other low z materials used, aluminum and carbon, instills some uncertainty in cavity theory at low energies. Just as Spencer and Attix (1955) discovered that δ rays significantly affected the doses at low energies, perhaps there is another process or interface phenomena which is causing this discrepancy.

The Burlin theory, as mentioned earlier, does not take into consideration any electron scattering. This as yet unknown exponential backscatter coefficient, $b(t)$, will have to be explored for better interpretations of cavity doses (Horowitz et al., 1986). The Burlin expression should be considered reasonably accurate only in the case of moderately mismatched cavity/medium interfaces where backscattering and other interface effects play a relatively insignificant role (Horowitz et al., 1986). It should be noted that

Horowitz et al. worked on comparing the fluences at the interface of the wall and cavity, and comparing the value of the electron mass fluence buildup coefficient, g , to the electron mass fluence attenuation coefficient, b . The study presented herein quantified f values for a cavity the size of a standard TLD chip for various wall media and a specific range of energies for comparison to the Burlin theory.

The much higher backscatter in the heavier elements and the lack of consideration for this factor in the theory, would seem to lend confidence to the hypothesis proposed herein. That is, the reason for the significant differences in f values for heavy elements is due to backscatter. This however, has not been proven and deserves further study. It is the opinion of this author that Burlin cavity theory, and its subsequent modifications, be used with caution when estimating a dose in a material with a severely different media than that of the sensitive volume inside the dosimeter. In light of the results and probable explanation found and described in this report, it is felt that this study has been a complete success which will prompt new investigations leading to the development of a system which will interpret doses in any media for any energy with minimal error.

FUTURE WORK

Obviously, the results of a single, small study should not be taken as the final word on the subject. However, these results do warrant further study. By using Monte Carlo techniques a backscatter coefficient should be investigated, as well as the expression in which d represents. The d equation should possibly be an integral over different densities and energies. These two parameters alone could significantly improve the accuracy of interpreting doses from TLD's for all media. Other continuing efforts could include separating out the backscatter to see exactly what kind of effect this has on the

cavity dose. A code could also be used to investigate interface interactions and effects at low energies to determine the cause for cavity doses lower than expected in the Burlin theory even for low Z media.

REFERENCES

- Attix, F.H. Introduction to radiological physics and radiation dosimetry. New York: John Wiley & Sons, Inc.; 1986.
- Bragg, W.H. Studies in radioactivity. New York: Macmillan; 1910.
- Burlin, T.E. A general theory of cavity ionisation. Br. J. Radiol. 39: 727; 1966.
- Burlin, T.E. Cavity - chamber theory. In: Attix, F.H.; Roesch, W.C., ed. Radiation dosimetry. New York and London: Academic Press; 1968.
- Burlin, T.E.; Chan, F.K. The energy - size dependence of the response of thermoluminescent dosimeters to photon irradiation. Health Phys. 18: 325; 1969.
- Gray, L.H. The absorption of penetrating radiation. Proc. Roy. Soc. A122: 647; 1929.
- Gray, L.H. An ionization method for the absolute measurement of g - ray energy. Proc. Roy. Soc. A156: 578; 1936.
- Harshaw / Filtrrol. Performance specifications. Harshaw / Filtrrol Partnership. Solon, Ohio.
- Horowitz, Y.S.; Moscovitch, M.; Mack J.M.; Hsu H.; Kearsley E. Incorporation of Monte Carlo electron interface studies into photon general cavity theory. Nuclear Science and Engineering. 94: 233; 1986.
- Kearsley, E. A new general cavity theory. Phys. Med. Biol. 29: 1179; 1984.
- Ogunleye, O.T.; Attix, F.H.; Paliwal, B.R. Comparison of Burlin cavity theory with LiF TLD measurements for cobalt - 60 gamma rays. Phys. Med. Biol. 25: 203; 1980.
- Paliwal, B.R.; Almond, P.R. Applications of cavity theories for electrons to LiF dosimeters. Phys. Med. Biol. 20: 547; 1975.
- Spencer, L.V.; Attix, F.H. A theory of cavity ionization. Radiation Research. 3: 239; 1955.
- Spencer, L.V. Note on the theory of cavity ionization chambers. Radiation Research. 25: 352; 1965.
- Spencer, L.V. Remarks on the theory of energy deposition in cavities. Acta Radiol. 10: 1; 1971.

Stanford Linear Accelerator Center, EGS4 A code system for the Monte Carlo simulation of electromagnetic cascade showers. Oak Ridge National Laboratory. RSIC Computer Code Collection, CCC - 331; 1986.

APPENDIX A

EGS4 SUBROUTINES

```

C*****
C*****
COMMON/BOUNDS/ECUT(20),PCUT(20),VACDST

COMMON/MEDIA/NMED,RLC(10),RLDU(10),RHO(10),MSGE(10),MGE(10),MSE
KE(
  *10),MEKE(10),MLEKE(10),MCMFP(10),MRANGE(10),IRAYLM(10)
COMMON/MEDIAC/MEDIA(24,10)
CHARACTER*4 MEDIA

COMMON/MISC/KMPI,KMPO,DUNIT,NOSCAT,MED(20),RHOR(20),IRAYLR(20)

COMMON/USEFUL/PZERO,PRM,PRMT2,RM,MEDIUM,MEDOLD,IBLOBE

COMMON/AS/TL(20,20,20),WALL(20,20,20)
COMMON/HF/A,B,C,AA,BB,CC,REGN,IRNXT
DOUBLE PRECISION PZERO,PRM,PRMT2
COMMON/STACK/E(40),X(40),Y(40),Z(40),U(40),V(40),W(40),DNEAR(40),W
*T(40),IQ(40),IR(40),NP
DOUBLE PRECISION E
C COMMONS NEEDED
c COMMON/LINES/NLINES,NWRITE
C TO KEEP TRACK OF LINES-PRINTED
COMMON/TOTALS/ESUM(20),TEMPW(20),TEMPT(20)
COMMON/RANDOM/IXX
c include in the upper line saf,coevr etc.
C FOR ENERGY CONSERVATION CHECK
DOUBLE PRECISION EI,ESUM,EKIN,TOTKE,ETOT
C DOUBLE PRECISION
C CREATE A TEMPORARY ARRAY AND DEFINE THE MEDIA, NEXT

CHARACTER*4 TEMP(24,7)/L',I',T',H',T',U',M',',
*'F',L',U',O',R',I',D',E',8*',
*'L',E',A',D',20*',A',L',U',M',T',N',U',M',16*',
*'F',E',22*',C',23*',C',U',22*',A',-',',1',5',0',
* 19*'/
INTEGER WALLMED
C LOCATED HERE TO AVOID FORTRAN 77 DIAGNOSTIC
open (unit = 12,file='INEGS.dat',status='old')
open (unit = 4, file='patcle.dat',status='old')
open (unit = 6, file='reslt.dat',status='new')
open (unit = 8, file='dummy.dat',status='new')
c file 12 is used in subroutine Hatch to obtain cross
c section data. It is used just one time.
c file 4 gives data related to particle characteristics
c and number of histories
c file 6 is the file used in Ausgab to obtain the neded
c saf, etc
c file 8 is used as a stored history cases to be run in Uphi

```

```

C STEP 2. PRE-HATCH-CALL-INITIALIZATION
NREG=3
C THE NUMBER OF REGIONS---A LOCAL VARIABLE ONLY
C TWO MEDIA WILL BE USED, VACCUM AND WATER
NMED=7
  DO 11 J=1,NMED
    DO 21 I=1,24
      MEDIA(I,J)=TEMP(I,J)
21 CONTINUE
11 CONTINUE
MED(3)=0
C REGION 2 MEDIUM
MED(2)=7 ! A-150
MED(1)=1 ! 1 IS LIF
C SET ENERGY CUTOFFS FOR EACH REGION NEXT
  DO 31 I=1,NREG
    ECUT(I)=.5210
    PCUT(I)=.001
31 CONTINUE
C
C STEP 3. HATCH-CALL
CALL HATCH
C
C STEP 4. INITIALIZATION-FOR-HOWFAR
C
C STEP 5. INITIALIZATION-FOR-AUSGAB
C
  DO 41 I=1,20
    ESUM(I)=0.D0
41 CONTINUE
C
C STEP 6. DETERMINATION-OF-INCIDENT-PARTICLE-PROPERTIES
C
  ESTEPE = ISTEP/100.0
  DO 77 MEDIUM =1,NMED
    CALL FIXTMX(ESTEPE,MEDIUM)
77 CONTINUE
C INCIDENT ENERGY EI (TOTAL) IN MEV
PRM =0.5110034
IF (IQI.EQ.-1) THEN
  EKIN=EI-PRM
ELSE
  EKIN = EI
ENDIF
C K.E. OF ELECTRON---PRM IS THE REST MASS
A =0.4511
B =0.5616
C =0.5616

```

```

AA =0.0445
BB =0.155
CC =0.155
READ(4,*)IQI,EI,NCASES,ISTEP
IXX=987654321
C   IXX IS A RANDOM NUMBER SEED
XI = - A + 0.000001
C   YI = 2*RAN(IXX)*B - B
C   ZI = 2*RAN(IXX)*C - C
C   XI = 0.0
C   YI = 0.0
C   ZI = 0.0
C   IRI = 2
C   COORDINATES OF INCIDENT PARTICLE
C
WTI=1.0
C   WEIGHT FACTOR---NOT USED IN CALCULATION, BUT
C   IS A PARAMETER IN SUBROUTINE SHOWER; HENCE DEFINE
C
AS UNITY
ICODE =-1
C   ICODE IS AN OUTPUTING PARAMETER, INVENTED TO MARK THE
C   INCIDENT PARTICLES
C   STEP 7. SHOWER-CALL
C
DO 61 I=1,NCASES
  WI = 0.0
  VI = 0.0
  UI = 1.0
  CALL SHOWER(IQI,EI,XI,YI,ZI,UI,VI,WI,IRI,WTI)
C   END OF SHOWER-CALL LOOP
61 CONTINUE
C
C   STEP 8. OUTPUT-OF-RESULTS
TOTKE=NCASES*EKIN
C   TOTAL K.E. INVOLVED IN RUN
C
C   CALCULATE AND PRINT OUT THE FRACTION OF ENERGY
C   DEPOSITED IN EACH REGION
ETOT=0.D0
C
DO 94 J=10,20,10
  DO 93 IX=J-9,J
    WRITE(6,81) IX
81  FORMAT(' TX = ',I3,J)
  DO 92 IZ= 1,20
    WRITE(6,82) (TLD(IX,I,IZ),I=1,20)
82  FORMAT(10(' ',F8.3)J,10(' ',F8.3)J)
  DO 91 IY=1,20

```

```

      ETLD=ETLD+TLD(IX,IY,IZ)
91 CONTINUE
92 CONTINUE
93 CONTINUE
94 CONTINUE
      DO 112 K = 10,20,10
      DO 110 IX = K-9,K
      WRITE(6,95) IX
95 FORMAT(' WX = ',I3,/)
      DO 105 IZ = 1,20
          WRITE(6,98) (WALL(IX,I,IZ),I=1,20)
98 FORMAT(10(' ',F8.3),/,10(' ',F8.3),/)
      DO 100 IY = 1,20
          EWALL = EWALL + WALL(IX,IY,IZ)
100 CONTINUE
105 CONTINUE
110 CONTINUE
112 CONTINUE
      ETOT = ETLD + EWALL
      RATIO = (ESUM(1)+ESUM(2))/ETOT
      WRITE(6,83) RATIO,ETOT,ESUM(1),ESUM(2),ESUM(3)
83 FORMAT(' RATIO = ',F10.8,' ETOT = ',F13.4,' ESUM(1) = ',F12.5,
      * / ESUM(2) = ',F13.4,' ESUM(3) = ',F13.4,/)
      DO 120 I = 1,20
      DO 118 IX = 1,20
      DO 116 IY = 1,20
          TEMPW(I) = TEMPW(I) + WALL(I,IX,IY)
          TEMPT(I) = TEMPT(I) + TLD(I,IX,IY)
116 CONTINUE
118 CONTINUE
      WRITE(6,119) I, TEMPW(I), I, TEMPT(I)
119 FORMAT(' SUM IN WALL LAYER ',I2,' = ',F10.4,/' SUM IN TLD
LAYER ',
      * I2,' = ',F10.4,/)
120 CONTINUE
      STOP
      END
C LAST STATEMENT OF MAIN

```

```

SUBROUTINE HOWFAR
COMMON/EPCONT/EDEP,TSTEP,TUSTEP,USTEP,TVSTEP,VSTEP,
IDISC,IROLD,IR
*NEW,RHOF,EOLD,ENEW,EKE,ELKE,BETA2, GLE,TSCAT,IAUSFL(25)

DOUBLE PRECISION EDEP
COMMON/STACK/E(40),X(40),Y(40),Z(40),U(40),V(40),W(40),DNEAR(40),W

```

```

*T(40),IQ(40),IR(40),NP
DOUBLE PRECISION E
C COMMON NEEDED IN HOWFAR
C SLAB THICKNESS DEFINED IN MAIN
COMMON/HF/A,B,C,AA,BB,CC,REGN,IRNXT
COMMON/RANDOM/IXX
REAL X1,X2,X3,X4,Y1,Y2,Y3,Y4,Z1,Z2,Z3,Z4
C
C INSIDE CAVITY

IF(ABS(X(NP)).LT.AA.AND.ABS(Y(NP)).LT.BB.AND.ABS(Z(NP)).LT.CC)THEN
    REGN=1
    IRNXT = 2
    IR(NP) = 1
C INSIDE WALL
ELSE

IF(ABS(X(NP)).LT.A.AND.ABS(Y(NP)).LT.B.AND.ABS(Z(NP)).LT.C)THEN
    REGN=2
    IR(NP) = 2
C OUTSIDE BOTH
ELSE
    IR(NP) = 3
    REGN=3
    IDISC=1
    RETURN
ENDIF
ENDIF
IF(REGN.EQ.1)THEN
    CALL CAVITY(DCLOSE, DELTAR)
    DNEAR(NP) = DCLOSE
ELSE
    CALL WALL(DCLOSE, DELTAR)
    DNEAR(NP) = DCLOSE
ENDIF
IF(DELTAR.LE.USTEP)THEN
    USTEP=DELTAR
    IRNEW = IRNXT
    RETURN
ELSE
    RETURN
ENDIF
END
C
SUBROUTINE CAVITY(DCLOSE, DELTAR)
COMMON/STACK/E(40),X(40),Y(40),Z(40),U(40),V(40),W(40),DNEAR(40),W

*T(40),IQ(40),IR(40),NP
DOUBLE PRECISION E

```

```

COMMON/HF/A,B,C,AA,BB,CC,REGN,IRNXT
C  CALCULATION OF DNEAR (DCLOSE)
   DTX1 = AA - ABS(X(NP))
   DTY1 = BB - ABS(Y(NP))
   DTZ1 = CC - ABS(Z(NP))
   DTX2 = 2*AA - DTX1
   DTY2 = 2*BB - DTY1
   DTZ2 = 2*CC - DTZ1
   DCLOSE = MIN(DTX1, DTY1, DTZ1, DTX2, DTY2, DTZ2)
C  CALCULATION OF DELTAR
   DELSTEP = 0.001
   X2 = X(NP)
   Y2 = Y(NP)
   Z2 = Z(NP)
12 IF(ABS(X2).LT.AA.AND.ABS(Y2).LT.BB.AND.ABS(Z2).LT.CC)THEN
    STEP = STEP + DELSTEP
    X2 = X(NP) + STEP * U(NP)
    Y2 = Y(NP) + STEP * V(NP)
    Z2 = Z(NP) + STEP * W(NP)
    GO TO 12
ENDIF
STEP2 = STEP - DELSTEP
20 IF(ABS(STEP - STEP2).GT.5.0E-4)THEN
   STEP3 = (STEP + STEP2)/2
   X3 = X(NP) + STEP3 * U(NP)
   Y3 = Y(NP) + STEP3 * V(NP)
   Z3 = Z(NP) + STEP3 * W(NP)
   IF(ABS(X3).GT.AA.OR.ABS(Y3).GT.BB.OR.ABS(Z3).GT.CC)THEN
C     OUTSIDE OF THE BOUNDARY
       STEP = STEP3
       GO TO 20
   ELSE
C     INSIDE OF THE BOUNDARY
       STEP2 = STEP3
       GO TO 20
   ENDIF
ENDIF
DELTAR = STEP3
IRNXT = 2
RETURN
END
C  SUBROUTINE WALL(DCLOSE, DELTAR)
COMMON/STACK/E(40),X(40),Y(40),Z(40),U(40),V(40),W(40),DNEAR(40),W
*T(40),IQ(40),IR(40),NP
DOUBLE PRECISION E
COMMON/HF/A,B,C,AA,BB,CC,REGN,IRNXT
C  CALCULATION OF DNEAR (DCLOSE)
   DTX1 = A - ABS(X(NP))

```

```

DTY1 = B - ABS(Y(NP))
DTZ1 = C - ABS(Z(NP))
DTX2 = ABS(X(NP)) - AA
DTY2 = ABS(Y(NP)) - BB
DTZ2 = ABS(Z(NP)) - CC
DCLOSE = MIN(DTX1, DTY1, DTZ1, DTX2, DTY2, DTZ2)
C  CALCULATION OF DELTAR
   DELSTEP = 0.001
   X2 = X(NP)
   Y2 = Y(NP)
   Z2 = Z(NP)
30  STEP = STEP + DELSTEP
   CALL WHERE(X,Y,Z,AUX)
   IF(AUX.EQ.2)THEN
       X2 = X(NP) + STEP * U(NP)
       Y2 = Y(NP) + STEP * V(NP)
       Z2 = Z(NP) + STEP * W(NP)
       GO TO 30
   ENDIF
   CALL WHERE(X2,Y2,Z2,AUX)
   IRNXT = AUX
   STEP2 = STEP - DELSTEP
40  IF(ABS(STEP - STEP2).GT.5.0E-4)THEN
       STEP3 = (STEP + STEP2)/2
       X3 = X(NP) + STEP3 * U(NP)
       Y3 = Y(NP) + STEP3 * V(NP)
       Z3 = Z(NP) + STEP3 * W(NP)
       CALL WHERE(X3,Y3,Z3,AUX)
       IF(AUX.NE.2)THEN
           C      OUTSIDE OF THE BOUNDARY
             STEP = STEP3
             GO TO 40
           ELSE
           C      INSIDE OF THE BOUNDARY
             STEP2 = STEP3
             GO TO 40
           ENDIF
       ENDIF
       DELTAR = STEP3
       RETURN
       END
SUBROUTINE WHERE(X,Y,Z,REGION)
C  INSIDE CAVITY
  IF(ABS(X).LT.AA.AND.ABS(Y).LT.BB.AND.ABS(Z).LT.CC)THEN
      REGION=1
C  INSIDE WALL
  ELSE
      IF(ABS(X).LT.A.AND.ABS(Y).LT.B.AND.ABS(Z).LT.C)THEN

```



```

                REGION=2
C      OUTSIDE BOTH
                ELSE
                REGION=3
                ENDIF
        ENDIF
        RETURN
        END

SUBROUTINE AUSGAB(IARG)
        COMMON/EPCONT/EDEP, TSTEP, TUSTEP, USTEP, TVSTEP, VSTEP,
IDISC, IROLD, IR
        *NEW, RHOF, EOLD, ENEW, EKE, ELKE, BETA2, GLE, TSCAT, IAUSFL(25)

        DOUBLE PRECISION EDEP
        COMMON/STACK/E(40), X(40), Y(40), Z(40), U(40), V(40), W(40), DNEAR(40), W
        *T(40), IQ(40), IR(40), NP
        DOUBLE PRECISION E
C      COMMONS NEEDED IN AUSGAB
        COMMON/AS/TLD(20,20,20), WALL(20,20,20)
        COMMON/HF/A,B,C,AA,BB,CC,REGN,IRNXT
        COMMON/LINES/NLINES, NWRITE
C      TO KEEP TRACK OF LINES-PRINTED
        COMMON/TOTALS/ESUM(20)
C      FOR ENERGY CONSERVATION CHECK
        DOUBLE PRECISION ESUM
C      DOUBLE PRECISION
C
C      NEW AUSGAB BELOW

IF(ABS(X(NP)).LT.AA.AND.ABS(Y(NP)).LT.BB.AND.ABS(Z(NP)).LT.CC)THEN
        IR(NP) = 1
        ELSE
        IF(ABS(X(NP)).LT.A.AND.ABS(Y(NP)).LT.B.AND.ABS(Z(NP)).LT.C)THEN
                IR(NP) = 2
                ELSE
                IR(NP) = 3
                ENDIF
        ENDIF
        IF(IR(NP).EQ.1)THEN
                IX = INT(X(NP)/(2.0*AA/20.0) + 10.0+1.0)
                IY = INT(Y(NP)/(2.0*BB/20.0) + 10.0+1.0)
                IZ = INT(Z(NP)/(2.0*CC/20.0) + 10.0+1.0)
                TLD(IX,IY,IZ) = EDEP + TLD(IX,IY,IZ)
        ENDIF
        IF(IR(NP).EQ.2)THEN

```

```
IX = INT(X(NP)/(2.0*A/20.0) + 10.0+1)
IY = INT(Y(NP)/(2.0*B/20.0) + 10.0+1)
IZ = INT(Z(NP)/(2.0*C/20.0) + 10.0+1)
IF(IX.GT.20.OR.IY.GT.20.OR.IZ.GT.20)THEN
ENDIF
WALL(IX,IY,IZ) = EDEP + WALL(IX,IY,IZ)
ENDIF
ESUM(IR(NP)) = ESUM(IR(NP)) + EDEP
RETURN
END
C LAST STATEMENT OF SUBROUTINE AUSGAB
```

APPENDIX B

RESULT DATA

ALUMINUM:
0.5 MeV:

Wall Layer	Energy Deposited (MeV)	Cavity Layer	Energy Deposited (MeV)
1	22.00	1	16.87
2	45.65	2	17.43
3	51.86	3	15.94
4	49.23	4	13.28
5	42.42	5	15.44
6	44.62	6	16.71
7	9.44	7	17.27
8	0.07	8	16.42
9	0.02	9	17.99
10	0.25	10	19.81
11	0.16	11	16.44
12	0.19	12	16.76
13	0.17	13	17.07
14	8.90	14	16.96
15	44.14	15	16.92
16	42.61	16	15.72
17	41.93	17	14.44
18	43.85	18	15.88
19	43.52	19	14.57
20	41.78	20	16.33

1 MeV:

1	33.47	1	32.79
2	71.00	2	28.90
3	96.66	3	27.93
4	112.04	4	31.41
5	115.08	5	30.36
6	119.20	6	33.12
7	132.64	7	33.66
8	69.56	8	34.44
9	0.57	9	30.39
10	0.53	10	33.92
11	0.42	11	34.37
12	0.88	12	31.40
13	65.77	13	33.39
14	123.62	14	29.29
15	121.11	15	29.22
16	125.52	16	30.09
17	130.10	17	31.50
18	125.29	18	31.88
19	120.90	19	30.63
20	97.21	20	30.98

1.25 MeV:

1	47.46	1	41.24
2	102.15	2	39.14
3	152.08	3	39.59
4	177.94	4	36.21
5	197.60	5	38.32
6	206.19	6	38.47
7	202.18	7	40.51
8	209.55	8	39.42
9	16.89	9	35.96
10	0.97	10	37.91
11	1.79	11	36.68
12	16.50	12	37.39
13	191.03	13	35.07
14	184.60	14	34.44
15	188.30	15	35.96
16	208.19	16	36.13
17	199.03	17	36.28
18	196.75	18	36.98
19	188.12	19	36.66
20	152.74	20	36.72

1.5 MeV:

1	57.81	1	43.23
2	140.49	2	42.73
3	206.25	3	43.82
4	249.27	4	42.96
5	286.60	5	45.67
6	293.55	6	44.84
7	294.14	7	43.45
8	276.55	8	41.67
9	128.93	9	41.71
10	3.21	10	42.28
11	3.68	11	40.84
12	137.68	12	42.11
13	290.95	13	41.59
14	273.23	14	40.44
15	286.51	15	40.70
16	278.26	16	40.47
17	253.24	17	45.61
18	253.48	18	41.66
19	247.91	19	42.68
20	234.70	20	44.71

CARBON
0.5 MeV:

1	21.58	1	13.91
2	39.82	2	13.58
3	42.16	3	16.39
4	43.91	4	17.17
5	48.65	5	15.32
6	47.03	6	15.00
7	34.46	7	15.45
8	0.10	8	15.60
9	0.08	9	14.17
10	0.06	10	13.71
11	0.21	11	14.54
12	0.29	12	14.60
13	0.44	13	15.76
14	29.92	14	15.09
15	41.89	15	14.74
16	38.86	16	15.51
17	42.26	17	15.51
18	44.76	18	15.43
19	43.64	19	13.84
20	42.31	20	12.48

1 MeV:

1	41.87	1	28.26
2	76.34	2	29.70
3	104.26	3	26.30
4	128.87	4	25.96
5	126.25	5	25.40
6	133.29	6	30.47
7	134.14	7	28.35
8	123.90	8	28.29
9	0.88	9	30.03
10	0.18	10	30.88
11	0.66	11	29.64
12	1.52	12	29.50
13	123.84	13	29.12
14	138.31	14	30.12
15	134.62	15	27.62
16	131.78	16	28.39
17	138.45	17	28.44
18	133.27	18	26.56
19	127.54	19	26.90
20	111.16	20	25.15

1.25 MeV:

1	56.28	1	32.00
2	106.88	2	35.04
3	139.87	3	33.90
4	189.89	4	35.84
5	207.99	5	30.43
6	203.00	6	33.37
7	204.87	7	33.49
8	208.65	8	34.13
9	83.12	9	35.27
10	1.88	10	29.98
11	2.26	11	30.71
12	93.48	12	30.15
13	211.32	13	30.54
14	205.10	14	31.20
15	212.01	15	28.04
16	213.51	16	30.08
17	205.74	17	34.84
18	203.31	18	32.67
19	211.45	19	30.93
20	203.55	20	30.02

1.5 MeV:

1	73.94	1	39.15
2	147.26	2	37.08
3	201.35	3	36.46
4	258.69	4	36.54
5	268.21	5	35.57
6	300.07	6	36.38
7	298.27	7	33.92
8	295.06	8	32.08
9	216.81	9	38.47
10	3.38	10	35.57
11	4.22	11	37.60
12	205.50	12	33.44
13	279.70	13	35.80
14	317.73	14	32.91
15	298.71	15	38.04
16	280.60	16	34.03
17	285.09	17	35.08
18	287.79	18	32.27
19	294.72	19	32.00
20	271.34	20	37.95

A - 150:
0.5 MeV:

1	16.31	1	7.75
2	31.47	2	7.74
3	35.53	3	9.07
4	41.88	4	8.12
5	38.71	5	7.69
6	42.53	6	8.67
7	45.66	7	7.83
8	39.57	8	7.48
9	0.23	9	8.58
10	0.35	10	9.12
11	0.37	11	8.17
12	0.09	12	7.89
13	39.02	13	7.62
14	41.08	14	7.46
15	39.34	15	7.16
16	40.30	16	7.68
17	38.75	17	8.34
18	37.66	18	9.11
19	41.33	19	9.02
20	41.22	20	8.26

1 MeV:

1	22.64	1	14.10
2	62.66	2	13.19
3	87.43	3	14.17
4	111.75	4	12.69
5	116.34	5	14.24
6	119.95	6	13.41
7	115.35	7	13.85
8	122.84	8	14.47
9	98.43	9	14.69
10	1.97	10	13.92
11	1.97	11	15.15
12	105.54	12	14.40
13	128.16	13	15.70
14	121.90	14	14.94
15	123.90	15	14.66
16	118.86	16	15.65
17	126.82	17	14.74
18	122.56	18	14.59
19	125.19	19	14.51
20	127.28	20	14.89

1.25 MeV:

1	33.07	1	17.89
2	87.27	2	18.81
3	126.16	3	18.44
4	147.66	4	19.31
5	164.49	5	17.96
6	182.61	6	18.93
7	179.50	7	17.92
8	185.87	8	17.73
9	188.07	9	16.52
10	13.88	10	18.78
11	12.99	11	16.66
12	185.15	12	16.58
13	177.42	13	18.64
14	187.20	14	17.30
15	186.73	15	17.50
16	192.19	16	18.47
17	180.45	17	16.50
18	187.65	18	17.01
19	179.52	19	16.87
20	161.74	20	17.64

1.5 Mev:

1	55.53	1	17.39
2	131.33	2	17.67
3	185.13	3	16.97
4	241.98	4	17.76
5	256.20	5	16.76
6	273.23	6	17.28
7	285.40	7	16.65
8	292.74	8	15.93
9	307.26	9	16.98
10	115.70	10	17.34
11	121.94	11	16.58
12	288.73	12	17.88
13	289.21	13	18.55
14	295.37	14	16.95
15	290.92	15	16.82
16	295.01	16	16.73
17	287.94	17	18.41
18	287.82	18	19.23
19	292.90	19	17.75
20	273.56	20	16.53

COPPER:
0.5 MeV:

1	66.35	1	54.80
2	87.63	2	58.85
3	86.89	3	57.68
4	27.32	4	56.92
5	0.50	5	60.07
6	0.27	6	57.33
7	0.18	7	60.17
8	0.34	8	55.62
9	0.32	9	59.50
10	0.22	10	58.41
11	0.24	11	60.13
12	0.32	12	60.37
13	0.45	13	60.78
14	0.58	14	58.39
15	0.19	15	55.65
16	0.52	16	60.66
17	25.16	17	56.91
18	89.70	18	54.53
19	95.41	19	56.82
20	86.53	20	54.98

1 MeV:

1	91.29	1	99.86
2	169.94	2	104.60
3	182.24	3	103.18
4	196.30	4	98.80
5	170.79	5	95.50
6	0.20	6	100.62
7	0.77	7	108.72
8	1.07	8	100.74
9	0.22	9	98.62
10	0.39	10	104.78
11	0.94	11	102.40
12	0.69	12	99.49
13	0.58	13	108.75
14	1.19	14	110.44
15	1.00	15	105.79
16	164.43	16	101.10
17	197.60	17	109.68
18	198.77	18	108.00
19	191.50	19	103.70
20	166.66	20	98.19

1.25 MeV:

1	119.28	1	129.78
2	225.64	2	133.29
3	265.70	3	129.82
4	297.80	4	122.13
5	294.10	5	120.63
6	187.11	6	117.68
7	0.97	7	116.93
8	1.60	8	120.46
9	0.70	9	120.19
10	1.32	10	118.19
11	0.76	11	113.39
12	0.90	12	111.27
13	1.11	13	119.01
14	2.27	14	123.67
15	166.89	15	124.09
16	273.49	16	113.63
17	275.72	17	117.10
18	274.61	18	118.19
19	266.52	19	113.12
20	212.00	20	117.29

1.5 MeV:

1	132.25	1	143.70
2	279.47	2	139.59
3	347.01	3	143.49
4	375.07	4	136.01
5	370.62	5	132.47
6	377.63	6	145.48
7	87.12	7	141.58
8	1.80	8	143.52
9	1.35	9	141.80
10	1.68	10	139.98
11	2.21	11	135.75
12	1.71	12	141.72
13	3.07	13	127.13
14	74.66	14	129.38
15	359.21	15	126.86
16	373.27	16	142.85
17	385.30	17	139.61
18	350.73	18	146.12
19	333.66	19	139.78
20	298.84	20	130.26

LEAD:
0.5 MeV:

1	298.67	1	192.78
2	401.66	2	145.72
3	340.86	3	153.12
4	1.05	4	172.39
5	0.96	5	196.05
6	0.61	6	218.28
7	1.40	7	230.61
8	1.40	8	249.24
9	0.19	9	260.31
10	0.34	10	269.47
11	0.81	11	269.37
12	0.92	12	264.41
13	0.88	13	274.64
14	1.34	14	261.06
15	1.73	15	253.04
16	2.26	16	263.59
17	0.85	17	261.56
18	415.36	18	261.51
19	502.58	19	258.48
20	410.28	20	271.38

1 MeV:

1	193.92	1	190.04
2	295.58	2	177.50
3	326.14	3	153.10
4	325.37	4	164.56
5	3.73	5	149.73
6	1.98	6	136.92
7	2.41	7	137.41
8	1.91	8	149.74
9	1.57	9	156.76
10	1.81	10	154.15
11	1.64	11	160.38
12	3.14	12	168.59
13	1.25	13	154.52
14	0.81	14	161.77
15	1.89	15	165.55
16	2.23	16	174.12
17	349.31	17	176.32
18	410.67	18	181.15
19	411.85	19	186.44
20	320.25	20	186.21

1.25 MeV:

1	194.32	1	183.86
2	350.98	2	180.16
3	415.89	3	178.84
4	394.08	4	168.05
5	299.83	5	163.67
6	3.82	6	163.95
7	2.91	7	154.75
8	4.89	8	148.17
9	3.40	9	164.94
10	3.65	10	166.02
11	3.91	11	162.45
12	6.00	12	161.04
13	4.08	13	167.21
14	4.13	14	163.38
15	2.97	15	160.60
16	305.90	16	175.14
17	437.64	17	170.97
18	435.57	18	163.08
19	415.55	19	172.00
20	334.52	20	178.14

1.5 MeV:

1	220.65	1	211.67
2	425.32	2	206.26
3	484.18	3	197.98
4	490.87	4	186.24
5	487.50	5	168.41
6	186.01	6	160.41
7	5.21	7	165.36
8	5.51	8	175.75
9	6.17	9	168.82
10	4.69	10	183.67
11	6.62	11	204.51
12	8.39	12	202.21
13	7.71	13	197.94
14	5.36	14	198.91
15	167.89	15	185.87
16	435.53	16	194.87
17	484.81	17	187.34
18	499.08	18	198.09
19	522.47	19	182.49
20	371.89	20	177.44

VITA

Name: Mark Duffy Weyland

Birth date: March 12, 1966

Education: B.S. Radiological Health Engineering (ABET Accredited Engineering Degree) Texas A&M University - August 1988

Employment: Graduate Research Assistant, Texas A&M University, Sept. 1988 - Sept. 1989

Permanent Address: 6019 Warm Springs; Houston, Texas 77035